VI. MICROWAVE ELECTRONICS*

Prof. L. D. Smullin
Prof. H. A. Haus
Prof. S. Saito (Visiting Fellow)

A. Bers
R. M. Bevensee
P. Chorney
H. W. Fock†

C. Fried
T. Goblick
A. J. Lichtenberg

A. MODE COUPLING IN PERIODIC CAVITY CHAINS

This report outlines a mathematical method by which the properties of a periodic chain of cavities (Fig. VI-1) can be deduced from normal mode expansions. The method is similar to Slater's method for finding the impedance of a single cavity as a function of frequency (1).

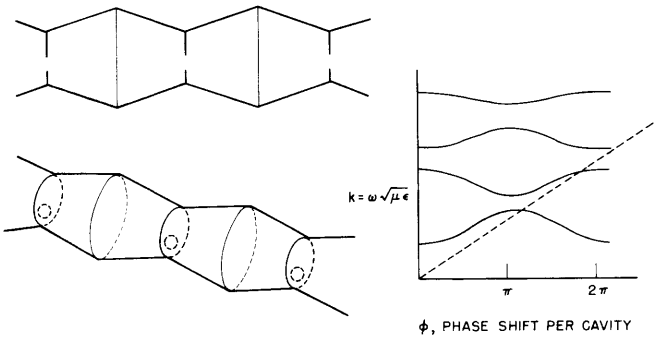

Fig. VI-1. Symmetrical cavity chain and its "ω-β" diagram.

Following Slater, we expand the fields within each cavity in a set of normalized resonant modes that are defined for each cavity with the coupling holes electrically shorted. Thus, we can represent the complex field vectors by an "electric" expansion:

$$\bar{E} = \sum_a V_a \bar{E}_a$$

$$\bar{H} = \sum_a I_a \bar{H}_a + \sum_a I'_a \bar{F}_a \qquad (1)$$

$$\nabla \times \bar{E} = \sum_a \left(P_a V_a \bar{H}_a + \int_s \bar{n} \times \bar{E} \cdot \bar{H}_a \, ds \right)$$

*This research was supported in part by Purchase Order DDL-B222 with Lincoln Laboratory, which is supported by the Department of the Army, the Department of the Navy, and the Department of the Air Force under Contract AF19(122)-458 with M. I. T.

†From Raytheon Manufacturing Company.

where P_a is Slater's k_a, the resonant frequency normalized with respect to the velocity of light.

However, such an expansion cannot represent the tangential electric field at the holes, so we also use a "magnetic" expansion, with resonant modes that are defined with the holes replaced by magnetic shorting planes. The magnetic modes will be denoted by lower-case letters. We have

$$\bar{E} = \sum_a v_a \bar{e}_a + \sum_a v'_a \bar{f}_a$$

$$\bar{H} = \sum_a i_a \bar{h}_a \tag{2}$$

$$\nabla \times \bar{H} = \sum_a \left(p_a v_a \bar{e}_a + \int_s \bar{n} \times \bar{H} \cdot \bar{e}_a \, ds \right)$$

The electric and magnetic expansions yield a determinantal equation for k^2 versus ϕ, the phase shift per cavity. With the fields at the holes appropriately expressed in a rapidly converging series, and the operating frequency very close to one of the magnetic and one of the electric mode resonances, but relatively far from the others, the determinantal equation can be simplified. The simplified equation gives good results, even for the configuration of Fig. VI-2, with a coupling hole that is one-quarter of the cross-section area.

To elaborate on these ideas, let us expand the fields in each cavity by Eqs. 1, using both even and odd modes, two of which appear in Fig. VI-3. The tangential fields at the holes converge rapidly if they are given by half of the sum of the fields on both sides. Thus, we have

$$\bar{E}|_{\text{hole}} = \frac{1}{2} \left(\sum_a [v_a \bar{e}_a + v'_a \bar{f}_a]_{\text{left side}} + \sum_a [v_a \bar{e}_a + v'_a \bar{f}_a]_{\text{right side}} \right) \tag{3}$$

$$\bar{H}|_{\text{hole}} = \frac{1}{2} \left(\sum_a [I_a \bar{H}_a]_{\text{left side}} + \sum_a [I_a \bar{H}_a]_{\text{right side}} \right) \tag{4}$$

These averages can be used because the expansions on both sides represent the same continuous field and hence are equivalent.

We write Maxwell's equations, using Eqs. 1, where $\bar{E}$ on the surface S, that is, the holes, is given by Eq. 3, and $\bar{H}$ on the surface is given by Eq. 4. To evaluate the amplitudes V_a, and I_a, we dot-multiply the $\nabla \times \bar{E}$-equation by $\bar{H}_a$, and the $\nabla \times \bar{H}$-equation by $\bar{E}_a$, and integrate them both over the volume. For frequencies close to the resonant

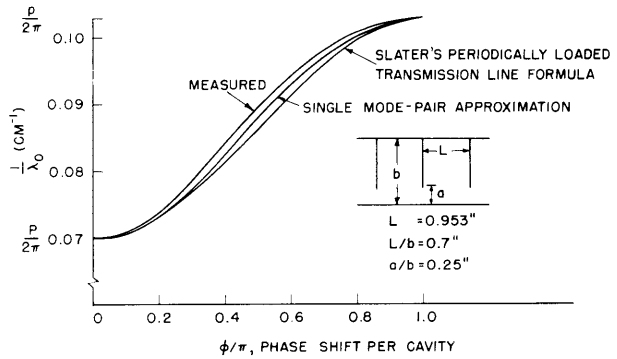

Fig. VI-2. Experimental and theoretical curves for the finned waveguide structure.

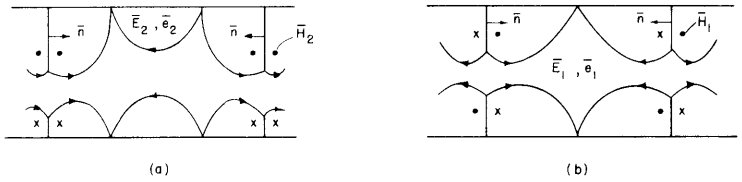

Fig. VI-3. Composite of (a) the second even electric and second even magnetic modes; (b) first odd electric and first odd magnetic modes.

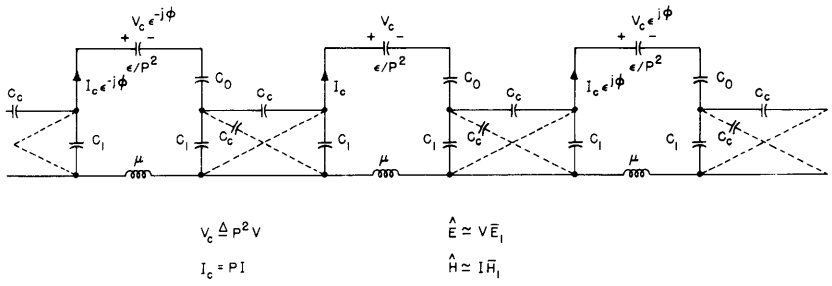

Fig. VI-4. Equivalent circuit for the single mode-pair approximation.
P, electric mode resonant frequency
Solid connections, odd mode
Dashed connections, even mode.

frequencies of an even electric- and a magnetic-mode pair, as shown in Fig. VI-3a, Maxwell's equations yield

$$P_e V_e = v_e M_e(1 - \cos \phi) - j\omega\mu I_e \tag{5a}$$

$$P_e I_e = j\omega\epsilon V_e \tag{5b}$$

with

P_e = normalized resonant frequency of the electric mode

ϕ = phase shift per cavity

$$M_e \triangleq \frac{1}{\text{volume}} \int_{\text{hole}} \bar{n} \times \bar{e}_e \cdot \bar{H}_e \, ds$$

The equivalent circuit, based on Eq. 5, appears in Fig. VI-4, in which C_1, C_c, and the series combination of ϵ/P^2 and C_o can all be made greater than zero. Combining Eqs. 5a and 5b, we obtain

$$\left(P_e^2 - k^2\right) V_e = P_e M_e v_e(1 - \cos \phi) \tag{6}$$

Another relation between V_e and v_e is implied by the equivalence of expansions 1 and 2 within the cavity for $\bar{E}$, but not for $\bar{H}$. In this approximation, it is

$$V_e \approx v_e \tag{7}$$

If we substitute this approximation in Eq. 6, together with the relation between M_e and the resonant frequencies which is found from one of Green's vector theorems,

$$P_e^2 - p_e^2 = 2P_e M_e \tag{8}$$

(where p_e is the magnetic mode resonant frequency), we obtain

$$\cos \phi = - \frac{P_e^2 - k^2 + p_e^2 - k^2}{P_e^2 - p_e^2} \tag{9}$$

Equation 9 states that at $k = P_e$, the electric resonance, ϕ, is zero, and, as a consequence, the tangential electric field at the holes is zero; at $k = p_e$, $\phi = \pi$, and the tangential magnetic field is zero.

If the analysis had involved frequencies close to the electric and magnetic resonances of an odd mode pair, Eq. 9 would become

$$\cos\phi = \frac{P_o^2 - k^2 + p_o^2 - k^2}{P_o^2 - p_o^2} \tag{10}$$

In approximate Eqs. 5 the fields in each cavity have been expanded in terms of the electric modes $\overline{E}_a$, $\overline{H}_a$, and $\overline{F}_a$. The excitation of these modes was computed from the tangential electric fields over the holes, which were found from the magnetic expansion. An alternative approach can start with an expansion of the fields inside each cavity in the magnetic modes $\overline{e}_a$, $\overline{h}_a$, and $\overline{f}_a$. Their excitation from the tangential magnetic fields across the holes can then be obtained from the electric expansion. The exact analysis, involving infinite expansions for the fields, leads to matrix relations analogous to Eqs. 5, 6, 7, and 8. The determinantal equation for k^2 versus ϕ is the same by either approach to the problem, except for a conjugate sign of k^2. But k^2 can be shown to be real by reciprocity arguments.

This work is presented more fully in a thesis that will be submitted to the Department of Electrical Engineering, M.I.T., in partial fulfillment of the requirements for the degree of Electrical Engineer.

R. M. Bevensee

References

1. J. C. Slater, Microwave Electronics (D. Van Nostrand Company, Inc., New York, 1950), Chap. 4.

B. DETERMINATION OF THE CORRELATION RATIO II/S OF THE NOISE IN AN ELECTRON BEAM

The system of measurement and the basic theory were outlined in the Quarterly Progress Report of July 15, 1957, page 52. The apparatus has been refined and measurements of the noise characteristics of two gun types were made: a simple, parallel-flow, single-anode Pierce gun; and the multi-anode gun used in the RCA low-noise, 10-cm, traveling-wave tube. Both guns had cathode diameters of 0.040 inch. Measurements were made at 3080 mc with a confining magnetic field of approximately 420 gauss. The interception current was approximately 0.05 per cent, and the pressure was approximately $2\text{-}4 \times 10^{-7}$ mm Hg.

The experiments will be described in Technical Report 333, Research Laboratory of Electronics, M.I.T. (to be published), so that only a summary of results will be given here. Measurements were made at varying times after initial cathode activation, and under both space-charge-limited and temperature-limited conditions. The results are summarized below.

	Space-charge-limited (watt-sec)	Temperature-limited (watt-sec)
RCA Gun No. 1	2 hours after activation	
	S $8.8 \times 10^{-21} \pm 8\%$	$1.22 \times 10^{-20} \pm 8\%$
	Π/S $0.21 \times 0.04\%$	$-0.02 \pm 0.04\%$
	80 hours after activation (cathode beginning to fail)	
	S $1.15 \times 10^{-20} \pm 8\%$	
	Π/S $-0.10 \pm 0.04\%$	
RCA Gun No. 2	10 hours after activation (cathode not yet fully activated)	
	Π/S $0.03 \pm 0.05\%$	
	50 hours after activation	
	S $9.42 \times 10^{-21} \pm 8\%$	$1.16 \times 10^{-20} \pm 8\%$
	Π/S $0.28 \pm 0.04\%$	$-0.13 \pm 0.04\%$
Parallel-Flow Gun	Π/S $0.26 \pm 0.06\%$	$0.04 \pm 0.08\%$

S. Saito

C. ELECTRON-STIMULATED ION OSCILLATORS

Work continues on both the theoretical and analytical aspects of electron-stimulated ion oscillations. The analytical approach is directed toward understanding the exact and approximate solutions of Maxwell's equations, for a waveguide filled with stationary ions and drifting electrons, in the presence of a finite, axial magnetic field. The experimental work is directed toward establishing some of the more important phenomena.

1. Theoretical Investigation of Electron-Stimulated Ion Oscillations

The system that was analyzed consisted of: (a) an electron beam of uniform dc charge density, $-\rho_o$, with drift velocity, $\vec{v}_o = \vec{i}_z v_o$, which is uniform across the beam cross section; (b) a cloud of positive ions of uniform dc charge density, $+\rho_o$, with zero drift velocity (trapped ions); (c) a focusing magnetic field, $\vec{B}_o = \vec{i}_z B_o$; and (d) a non-accelerating dc field, $\vec{E}_o = 0$. The electron beam drifts through the positive ion cloud; and since it is assumed that the beam and the ions occupy the same space, the net dc space-charge density is zero. The rf currents and charges caused by the motion of both the electrons and the ions were not neglected in Maxwell's equations.

The following equations were used to describe the system, variations of the

form $e^{j\omega t - j\beta_z z}$ being assumed:

$$\nabla^2 \vec{E} + k^2 \vec{E} = j\omega\mu\vec{J} + \frac{\nabla\rho}{\epsilon_o} \tag{1}$$

$$\nabla^2 \vec{H} + k^2 \vec{H} = -\nabla \times \vec{J} \tag{2}$$

$$\rho = \rho_o \left\{ \frac{\nabla \cdot \vec{v}_e}{j\omega\left(1 - \frac{\beta_z}{\beta_e}\right)} - \frac{\nabla \cdot \vec{v}_i}{j\omega} \right\} \tag{3}$$

$$\vec{J} = \rho_o \left\{ \vec{v}_i - \vec{v}_e + \frac{\nabla \cdot \vec{v}_e}{j\omega\left(1 - \frac{\beta_z}{\beta_e}\right)} \vec{v}_o \right\} \tag{4}$$

$$\frac{j\omega m_i}{q} \vec{v}_i = \vec{E} + \vec{v}_i \times \vec{B}_o \tag{5}$$

$$-\frac{j\omega m_e}{e}\left(1 - \frac{\beta_z}{\beta_e}\right)\vec{v}_e = \vec{E} + \vec{v}_e \times \vec{B}_o + \mu_o \vec{v}_o \times \vec{H} \tag{6}$$

where $\beta_e = \omega/v_o$, $k = \omega/c$, and $\vec{E}$, $\vec{H}$, ρ, $\vec{J}$, $\vec{v}_i$, $\vec{v}_e$ are rf quantities. Equations 1 and 2 were derived from Maxwell's equations. Equations 3 and 4 were obtained from the ion and electron continuity equations, with the assumption of small-signal theory. Equations 5 and 6 describe the motion of the ions and electrons, with the assumption of small-signal theory. The force on an electron caused by the rf magnetic field was considered; relativistic effects were ignored.

In rectangular coordinates the rf quantities were assumed to vary as $\exp(-j\beta_x x - j\beta_y y - j\beta_z z)$. The determinantal equation that relates β_x, β_y, β_z, ω, ρ_o, B_o, and v_o was obtained in the form of a sixth-order determinant equated to zero. The expansion of this determinant for the general case is rather complicated, but it has been expanded for a few special cases.

If we let $B_o = 0$ and $v_o = 0$, the sixth-order determinant can be expanded to give the following determinantal equation:

$$\left(1 - \frac{\omega_{pi}^2}{\omega^2} - \frac{\omega_{pe}^2}{\omega^2}\right)\left[-\beta_x^2 - \beta_y^2 - \beta_z^2 + k^2\left(1 - \frac{\omega_{pi}^2}{\omega^2} - \frac{\omega_{pe}^2}{\omega^2}\right)\right] = 0$$

This equation shows that if $\omega = \left(\omega_{pi}^2 + \omega_{pe}^2\right)^{1/2}$, then the choice of β_x, β_y, and β_z is arbitrary (as long as boundary conditions are satisfied). For $\omega \neq \left(\omega_{pi}^2 + \omega_{pe}^2\right)^{1/2}$, the propagation constant β_z is determined by the second factor.

For $B_o = \infty$, the determinantal equation is

$$-\beta_x^2 - \beta_y^2 + \left(-\beta_z^2 + k^2\right)\left[1 - \frac{\omega_{pi}^2}{\omega^2} - \frac{\omega_{pe}^2}{\omega^2}\frac{\beta_e^2}{(\beta_e - \beta_z)^2}\right] = 0$$

where $\omega_{pe}^2 = (e\rho_o)/\epsilon_o m_e$ and $\omega_{pi}^2 = (q\rho_o)/\epsilon_o m_i$. In this case the particles are constrained to move in the z-direction. β_x and β_y are determined by boundary conditions.

For the special case of one-dimensional variation, the expanded sixth-order determinant gives the following determinantal equation for the propagation constant β_z:

$$\left[\left(1 - \frac{\beta_z}{\beta_e}\right)^2\left(1 - \frac{\omega_{pi}^2}{\omega^2}\right) - \frac{\omega_{pe}^2}{\omega^2}\right]\left\{\left(1 - \frac{\beta_z}{\beta_e}\right)^2\left[-\beta_z^2 + \frac{\omega^2 - \omega_{pe}^2 - \omega_{pi}^2}{c^2}\right]^2\right.$$

$$- \frac{\omega_{ci}^2}{\omega^2}\left[\left(1 - \frac{\beta_z}{\beta_e}\right)^2\left(-\beta_z^2 + \frac{\omega^2 - \omega_{pe}^2}{c^2}\right)^2 - \frac{\omega_{ce}^2}{\omega^2}\left(-\beta_z^2 + k^2\right)^2\right]$$

$$- \frac{\omega_{ce}^2}{\omega^2}\left[-\beta_z^2 + \frac{\omega^2 - \omega_{pi}^2}{c^2}\right]^2$$

$$\left. + 2\,\frac{\omega_{ce}\omega_{ci}}{\omega^2}\frac{\omega_{pe}^2}{c^2}\frac{\omega_{pi}^2}{c^2}\left(1 - \frac{\beta_z}{\beta_e}\right)\right\} = 0 \qquad (7)$$

where $\omega_{ce} = (eB_o)/m_e$ and $\omega_{ci} = (qB_o)/m_i$. It can be shown that in this one-dimensional case, longitudinal and transverse motions of the particles can exist independently. The first factor of Eq. 7 gives the propagation constant for longitudinal motion of the particles,

$$\beta_z = \frac{\omega}{v_o} \pm \frac{\frac{\omega_{pe}}{v_o}}{\left(1 - \frac{\omega_{pi}^2}{\omega^2}\right)^{1/2}}$$

This is the same equation that was obtained by Pierce (1). The second factor gives the propagation constant when particle motion is excited transversely to the direction of propagation. For a system consisting only of ions, the one-dimensional solution for transverse oscillations becomes

$$\beta_z^2 = k^2 \left[1 - \frac{\frac{\omega_{pi}^2}{\omega^2}}{1 \pm \frac{\omega_{ci}}{\omega}} \right]$$

which is in agreement with Spitzer (2).

The problem of a rectangular waveguide filled with a cloud of positive ions of uniform dc charge density ρ_o in an axial magnetic field B_o was also investigated. In this problem the sixth-order determinant reduces to a third-order determinant, which is expanded to give the following determinantal equation:

$$\left[-\beta^2 + k^2 \left(1 - \frac{\omega_p^2}{\omega^2} \right) \right]^2 \left[1 - \frac{\omega_p^2}{\omega^2} \right] - \frac{\omega_c^2}{\omega^2} \left[-\beta^2 + k^2 \left(1 - \frac{\omega_p^2}{\omega^2} \right) + \frac{\omega_p^2}{\omega^2} \beta_z^2 \right] \left[-\beta^2 + k^2 \right] = 0 \qquad (8)$$

where $\omega_p^2 = \frac{q\rho_o}{\epsilon_o m_i}$, $\omega_c = \frac{qB_o}{m_i}$, $\beta^2 = \beta_x^2 + \beta_y^2 + \beta_z^2$; $\beta_x^2 = \left(\frac{\ell\pi}{x_o}\right)^2$, $\beta_y^2 = \left(\frac{m\pi}{y_o}\right)^2$, ℓ and m are positive nonzero integers, and x_o, y_o are the waveguide dimensions. Two waves, each of which can be forward- or backward-traveling, are predicted by Eq. 8. One wave is cut off, except at very high frequencies, and varies approximately as $\beta_z = \left(k^2 - \beta_x^2 - \beta_y^2\right)^{1/2}$. The other wave is either propagated or attenuated, as shown in Fig. VI-5 and in Fig. VI-6. The propagation constant of this wave has poles at ω_p and ω_c, and zeros at $\omega \approx \left(\omega_p^2 + \omega_c^2\right)^{1/2}$ and at $\omega \approx \left(\omega_p^2 + \beta_x^2 c^2 + \beta_y^2 c^2\right)^{1/2}$.

By assuming that $\nabla \times E = 0$, the following determinantal equation was obtained by using Poisson's equation in conjunction with the force and continuity equations.

$$\beta_z^2 = \frac{\omega^2\left(\omega_p^2 + \omega_c^2 - \omega^2\right)}{\left(\omega^2 - \omega_p^2\right)\left(\omega^2 - \omega_c^2\right)} \left(\beta_x^2 + \beta_y^2\right) \qquad (9)$$

The electromagnetic equation (Eq. 8) reduces to the electrostatic equation (Eq. 9) if we let k = 0. In the electrostatic case, $\beta_z \to j\left(\beta_x^2 + \beta_y^2\right)^{1/2}$ as ω goes to ∞, whereas in the electromagnetic solution $\beta_z \to \left(k^2 - \beta_x^2 - \beta_y^2\right)^{1/2}$ as ω goes to ∞. Moreover, the electrostatic case does not predict the high-frequency passband, since at high frequencies k is no longer negligible.

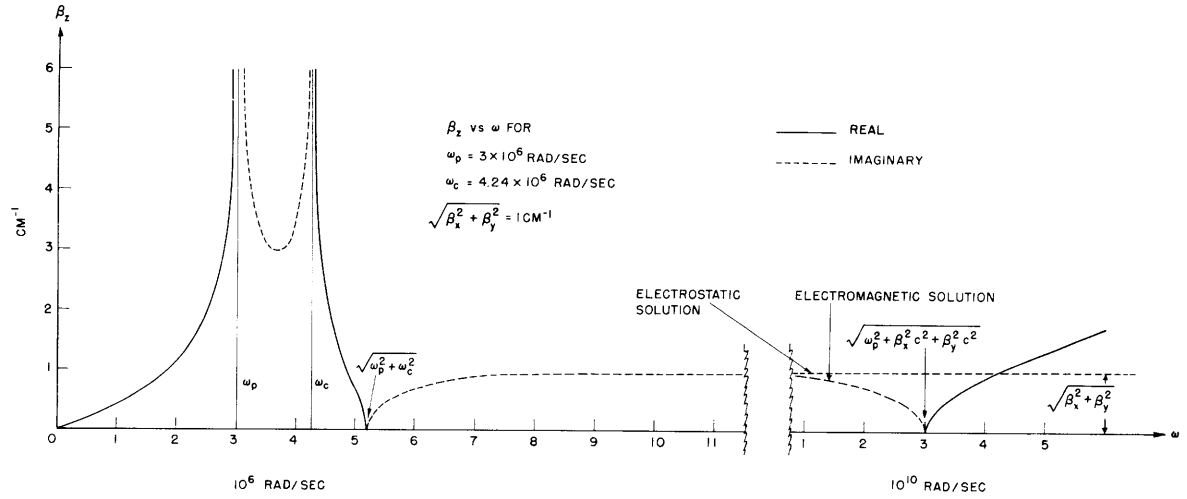

Fig. VI-5. β_z versus ω for $\omega_p < \omega_c$.

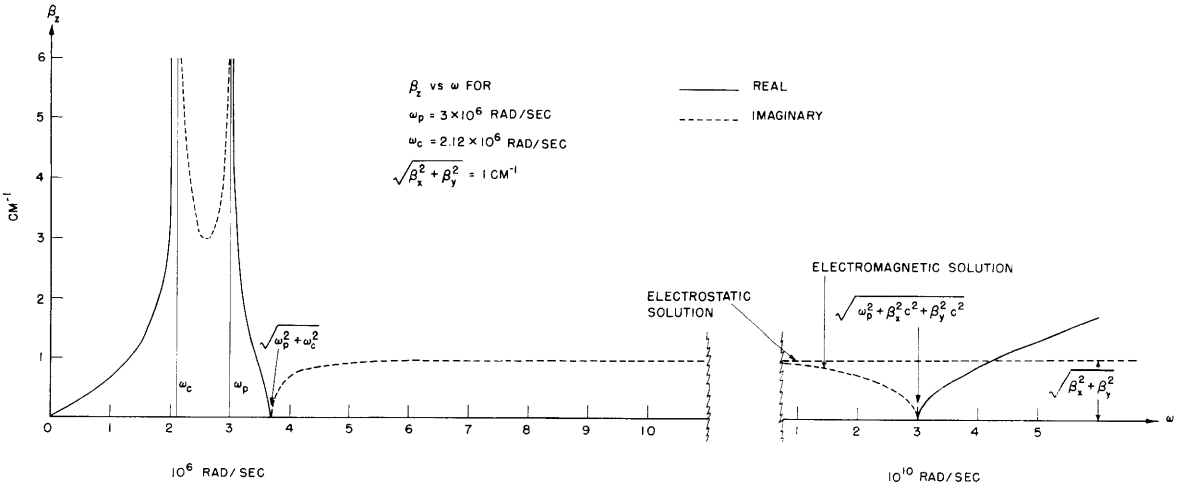

Fig. VI-6. β_z versus ω for $\omega_p > \omega_c$.

For the values chosen in Figs. VI-5 and VI-6, the electromagnetic and electrostatic plots of β_z against ω coincide very closely at low frequencies, where k is negligible, and do not coincide at high frequencies, where k is no longer negligible. The low-frequency cutoff, $\omega = \left(\omega_p^2 + \omega_c^2\right)^{1/2}$, is exact in the electrostatic case, and is a very good approximation in the electromagnetic case. In the electromagnetic case the high-frequency cutoff, $\omega = \left(\omega_p^2 + \beta_x^2 c^2 + \beta_y^2 c^2\right)^{1/2}$, is a very good approximation; this is essentially the same cutoff as in the empty waveguide.

P. Chorney

References

1. J. R. Pierce, Possible fluctuations in electron streams due to ions, J. Appl. Phys. 19, 231-236 (1948).
2. L. H. Spitzer, Jr., Physics of Fully Ionized Gases (Interscience Publishers, Inc., New York, 1956), Chap. 4, p. 53.

2. Experiments on Ion Oscillations in Electron Beams

The apparatus that is used is a continuously pumped system, described in the Quarterly Progress Report of April 15, 1957, page 51. A gun of perveance 0.8×10^{-6} was used in approximately confined flow (the flux through the cathode was roughly equal to the flux through the drifting beam). It was possible to admit various gases at controlled pressure, but all of the experiments reported here were made with hydrogen. The experiments are still exploratory and represent an attempt to find points of correspondence between theory and experiment.

Figure VI-7 is a schematic of the apparatus, showing the electrodes and metering arrangements. The drift tubes D_1 and D_2 had an inside diameter of 5/8 inch and were 8 inches long. The beam diameter was approximately 0.2 inch. A typical dc potential profile is shown, in which V_o is the anode-cathode accelerating voltage. Within the cathode structure and back of the cathode, a probe system was arranged to measure particle current flowing toward the cathode and through the hole.

Figure VI-8 illustrates the limiting perveance obtainable under so-called ion-neutralized conditions. V_o was held fixed at the indicated values, and V_D was varied. The plot of $I^{2/3}$ vs. $(V_o - V_D)$ corresponds to the perveance of the drifting beam. Several features are noteworthy: as $(V_o - V_D)$ is reduced, most of the curves begin to droop immediately, and finally, at the value of $(V_o - V_D)$ corresponding to a perveance of approximately 10^{-5}, there is a sudden break in the current. If we compute the limiting perveance of an unneutralized beam (radius b) in a drift tube (radius $a \approx 3b$), which is confined by a strong magnetic field, we find almost the same value as that of our experiments. Thus we see that although a relatively efficient ion trap was provided, there was no increase in the limiting perveance as compared with a pure electron beam (1).

The uppermost curves in Fig. VI-8 ($V_o = 2050$) show a temperature-limited curve that is almost flat down to the break. This seems to allow the hypothesis that electrons are being accelerated back into the gun region. If they reach the cathode, the net current I_c is reduced by the algebraic sum of the forward and backward currents. If the gun is space-charge-limited, the backward current exerts an additional influence by reducing the forward current; but this additional effect is not present in a temperature-limited gun. (It should be noted that when D_1, the drift tube near the cathode, was held

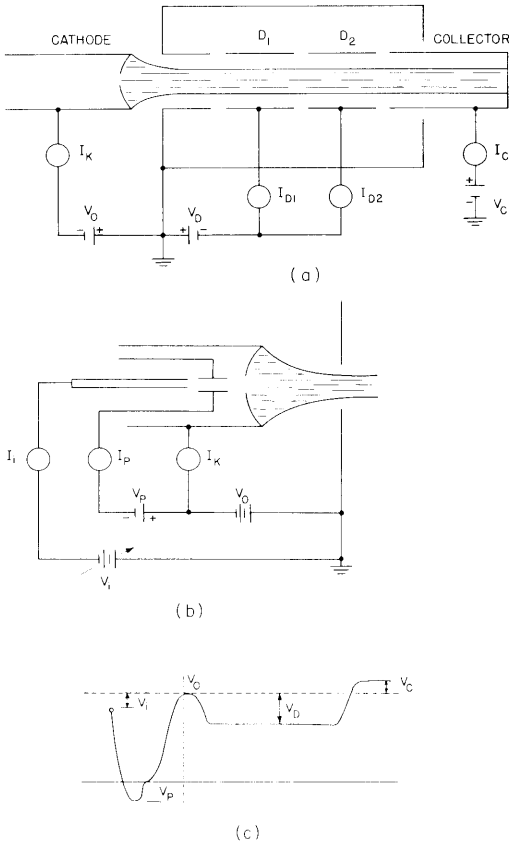

Fig. VI-7. (a) Apparatus for observing the behavior of an ion-neutralized electron beam. An axial magnetic field through the cathode is used to focus the beam. (b) Probe arrangement behind the cathode. (c) Axial potential profile through the system.

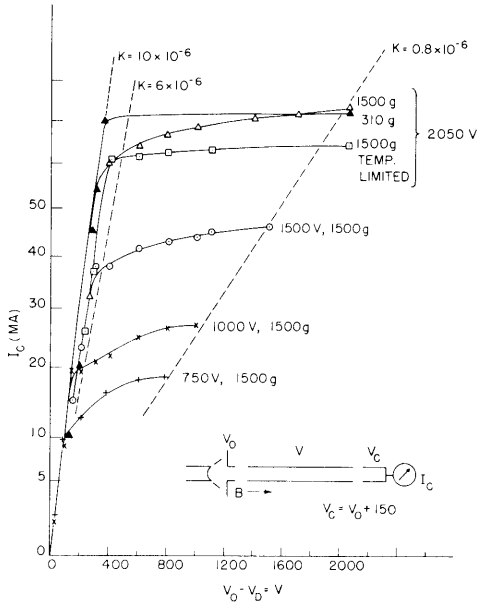

Fig. VI-8. Curves illustrating the limiting perveance of an ion-neutralized beam. The perveance is defined as $K = I_c/V^{3/2} = I_o/(V_o - V_D)^{3/2}$.

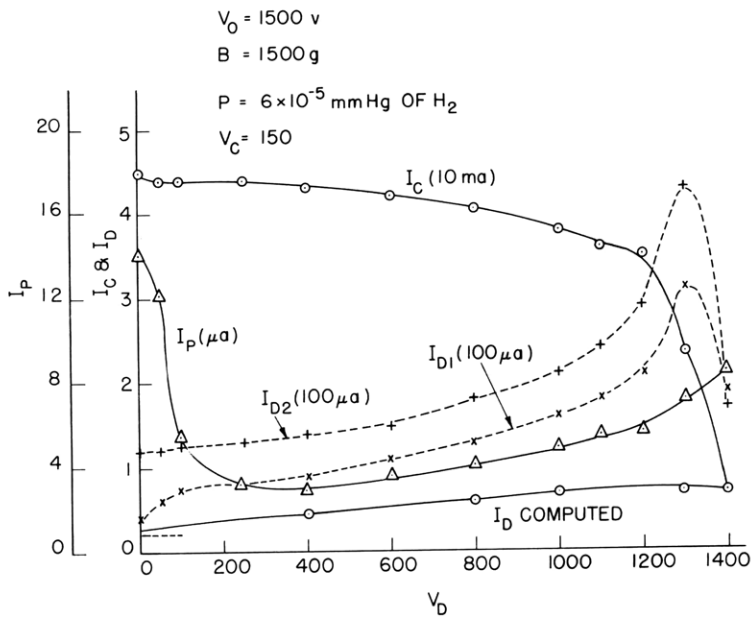

Fig. VI-9. Currents flowing in the apparatus of Fig. VI-7 plotted against V_D.

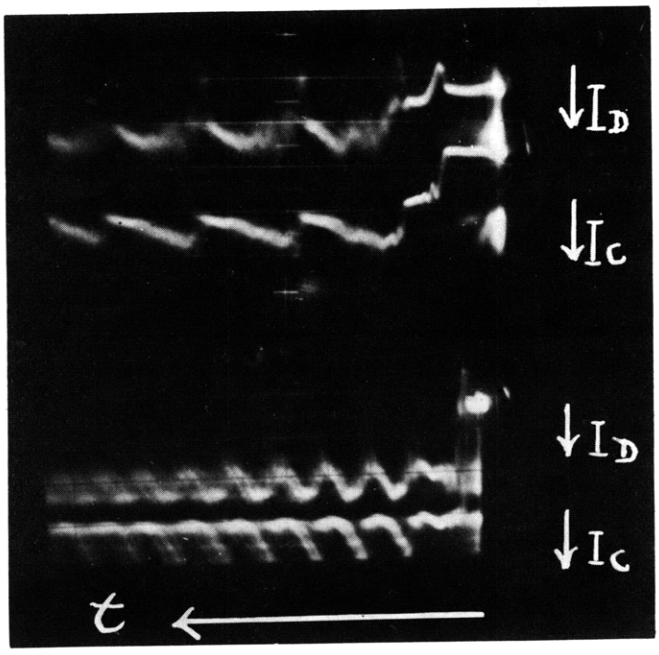

Fig. VI-10. Relaxation oscillations in collector I_c and drift-tube I_c currents. Increasing current is indicated downward; time, toward the left.

at V_o, all of the curves became flat until critical perveance was reached.)

Figure VI-9 shows several currents as functions of the drift-tube potential V_D (when $V_D = 0$ the beam is drifting at a potential V_o). The ion current to the probe in back of the cathode, I_p, is interesting in that it is not cut off by the trapping voltage V_D (see ref. 2). This anomalous current is tentatively taken as evidence that strong ion oscillations within the drift-tube region may eject some ions with enough energy to climb over the trapping potential barriers.

The currents I_{D1} and I_{D2} are of the proper sign for positive ion currents. However, if we use the appropriate ionizing cross section (3) for hydrogen, the computed curve, I_D computed, is lower than either I_{D1} or I_{D2} by a factor of 3 or 4. The most plausible explanation is that the beam electrons do not travel in straight lines, but that they acquire sufficient transverse motion to give them a longer effective ionizing path length.

Oscillations were observed by connecting either a wideband oscilloscope or a spectrum analyzer to the collector or to the drift tubes. We observe two main classes of oscillation, after insuring that no electrons are allowed to return to the gun from the collector: (a) a nearly sinusoidal oscillation of 1-2 mc, and (b) a relaxation oscillation with a frequency in the tens to hundreds of kilocycles per second. The sinusoidal oscillations in collector current appear to be an "ion plasma oscillation," in that the frequency is primarily associated with electron current density, although it was always smaller than the computed frequency for a fully neutralized beam by a factor of 2 or 3. This might be taken to indicate that the beam is only 10-25 per cent neutralized, which would not be inconsistent with the results of Fig. VI-8. By means of a probe that could be moved across the beam, it was established that the beam bulges periodically at the observed frequency.

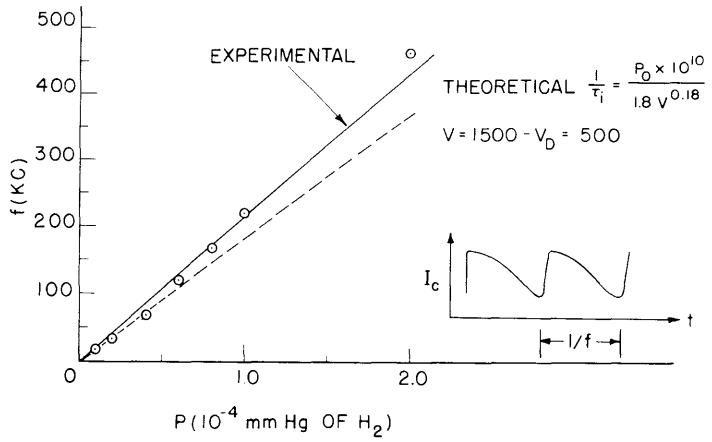

Fig. VI-11. Plot of relaxation oscillation frequency against ambient gas pressure. Insert, computed curve of (ionization time)$^{-1}$, $1/\tau_i$.

In addition to the sinusoidal oscillations, when V_D exceeds several hundred volts, relaxation oscillations of the type shown in Fig. VI-10 are observed. They may be seen in the collector, cathode, or drift-tube currents. They are very stable and reproducible. No explanation exists for them, but Fig. VI-11 may indicate something of their nature. Here we plotted the frequency of these oscillations against the ambient gas pressure; the dotted line is the theoretical curve of $1/\tau_i$, where τ_i is the time required to fully neutralize the beam (4). Since these oscillations are observable in the cathode current, and since the collector-current oscillations seem to be downward from the nonoscillating current level, we may associate the relaxation oscillations with the drooping characteristic of Fig. VI-8 that has already been tentatively explained on the basis of electrons returning to the cathode.

L. D. Smullin, C. Fried

References

1. An experiment performed by Hollenberg gives similar results; cf. J. R. Pierce, Theory and Design of Electron Beams (D. Van Nostrand Company, Inc., New York, 1949).
2. Similar data are shown in Fig. 6 of J. P. Laico, H. L. McDowell, and C. R. Moster, A medium power traveling wave tube for 6000 Mc radio relay, Bell System Tech. J. 35, 1285 (1956).
3. S. C. Brown and W. P. Allis, Basic data of electrical discharges, Technical Report 283, Third Edition, Research Laboratory of Electronics, M.I.T., Sept. 1, 1956.
4. Coefficients are taken from S. C. Brown and W. P. Allis, op. cit.

D. MULTICAVITY KLYSTRONS*

1. Theory: Cavities with Gaps of Finite Length

The small-signal multicavity-klystron theory (1) that has been presented thus far has assumed that the cavity gaps are of infinitesimal length, and has taken account of electronic loading only. Broadband multicavity klystrons must make use of cavities whose gaps are appreciably long (2). We propose to investigate the effect of a finite gap with reference to the small-signal behavior of broadband multicavity klystrons.

Assume that the fields in the finite gap are quasi-static and that space-charge effects within the gap are negligible. Partial justification for these assumptions comes from noting that the 2-radian gaps of the proposed tube (2) have the following characteristics:

*This work was supported in part by the Office of Naval Research under Contract Nonr 1845(05).

$$\left.\begin{aligned} d &\approx \frac{\lambda/4}{1.8} \\ d &\approx \frac{\lambda_q/4}{6.3} \end{aligned}\right\} \tag{1}$$

where d is the gap length, λ is the operating wavelength, and λ_q is the corrected plasma wavelength. Under these assumptions, the effect of a cavity upon a modulated electron beam that passes through its gap can be represented by a linear two-port transformation of the kinetic voltage and total current (3):

$$\begin{pmatrix} V_2 \\ I_2 \end{pmatrix} = \begin{pmatrix} A_g & Z_g \\ Y_g & A_g \end{pmatrix} \begin{pmatrix} V_1 \\ I_1 \end{pmatrix} \tag{2}$$

in which we have abbreviated as follows:

$$A_g = y_5 + a\, y_4 = y_5 - y_4 Y_2 Z \tag{3}$$

$$Z_g = y_4^2 \frac{a}{Y_2} = -y_4^2 Z \tag{4}$$

$$Y_g = Y_3 + a Y_2 = Y_3 - Y_2^2 Z \tag{5}$$

and the definitions of all quantities are given in reference 3. (Note an error in ref. 3: $y_5 = e^{-j\theta/2}$ should read $y_5 = e^{-j\theta}$.) Each term in Eqs. 3, 4, and 5 represents a distinct physical process in the gap. Hence it will be found convenient to use flow-graph techniques in making approximations and in evaluating such systems with relative ease. The finite-gap equations can be broken up conveniently, as shown in Fig. VI-12. The first graph on the right-hand side of the topological equation in Fig. VI-12 is readily recognized as being the representation of the infinitesimal gap, except that the actual gap transit angle is explicitly contained. Hence the last graph of Fig. VI-12 contains all the effects of the finite gap that have been neglected in the infinitesimal-gap theory.

Let us represent the drift regions between cavities by the two-port (single-mode) space-charge equation

$$\begin{pmatrix} V_2 \\ I_2 \end{pmatrix} = \begin{pmatrix} A_d & Z_d \\ Y_d & A_d \end{pmatrix} \begin{pmatrix} V_1 \\ I_1 \end{pmatrix} \tag{6}$$

where

$$A_d = \cos\theta \tag{7}$$

$$Z_d = j Z_o \sin\theta \tag{8}$$

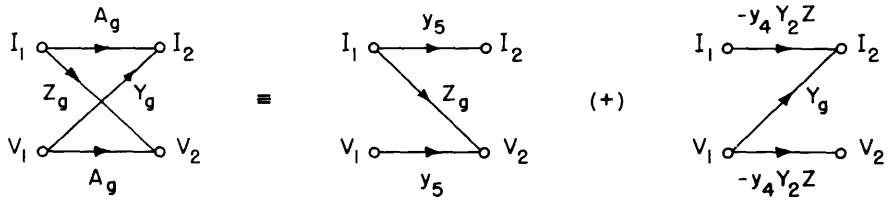

Fig. VI-12. Finite-gap equations in flow-graph form. The sign (+) indicates that similar nodes are coincident.

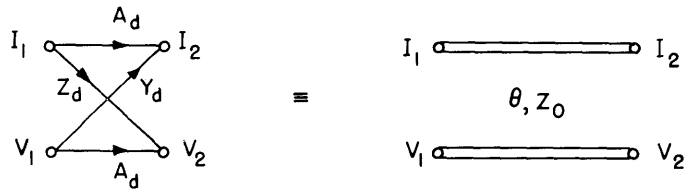

Fig. VI-13. Drift-region equations in flow-graph form and an abbreviated representation.

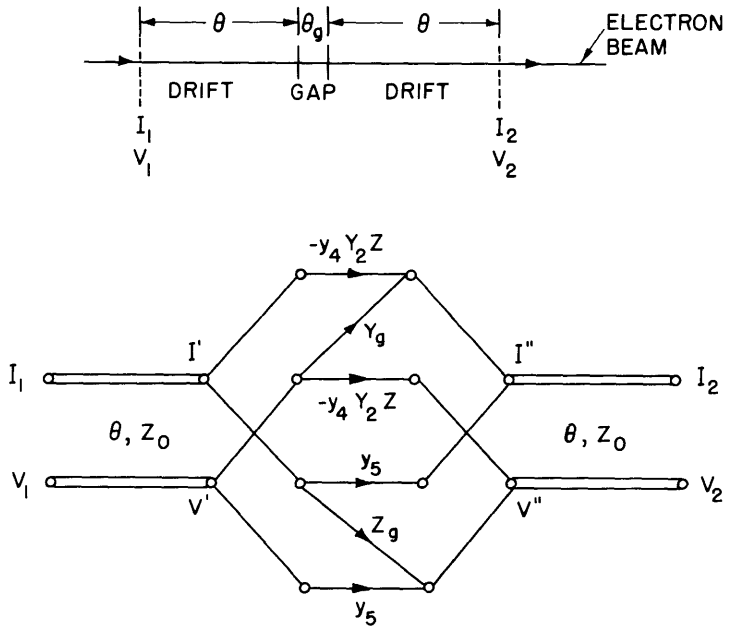

Fig. VI-14. Prototype of multicavity-klystron structure and its flow-graph representation. Single lines without arrows have unity transmission.

$$Y_d = j\, Y_o \sin\theta \tag{9}$$

θ represents the corrected plasma transit angle of the drift region, and $Z_o = 1/Y_o$ is the characteristic impedance of the drifting beam. Because of the similarity of these equations to those of a lossless transmission-line section, we choose the representation as shown in Fig. VI-13.

With these formulations, the prototype section of a multicavity klystron – a gap preceded and followed by drifts – can be conveniently represented as shown in Fig. Fig. VI-14. Suppose the entering beam has a kinetic voltage V_1, and we wish to find the resulting output current I_2. The result is

$$\left.\frac{I_2}{V_1}\right|_{I_1=0} = \left(Y_o^2 \sin^2\theta\, M^2 Z + j\, Y_o \sin 2\theta\right) e^{-j\theta_g} + \cos^2\theta\, Y_g - j\, Y_o \sin 2\theta\, y_4\, Y_2\, Z \tag{10}$$

The terms in brackets are the usual short-gap cascade and feedforward terms that can be obtained by inspection (1) by considering the lower part of the gap graph. The two additional terms are similar in nature to a cascade and a feedforward (modified by a finite gap) term, as evidenced by the upper part of the gap graph. The extension of these ideas to a multigap problem is obvious.

2. Theory: Approximations in Finite-Gap Equations

Consider the 2-radian cavity gaps of the proposed tube (2). The gap parameters, at resonance, are found to be

$$Z_g = 2.54 \times 10^3 \angle -115.6^\circ \quad \text{ohms}$$

$$y_5 = 1.0 \angle 65.4^\circ$$

$$Y_g = 2.64 \times 10^{-3} \angle -115^\circ \quad \text{mhos}$$

$$-y_4 Y_2 Z = 2.95 \angle 135^\circ$$

The beam characteristic impedance is $Z_o = 113$ ohms. This example indicates that the only significant effect that the short-gap theory neglects is the remodulation of the current I', which enters the gap, into I" through the gap impedance. This effect is significant in magnitude and is frequency-dependent. It is also easily seen that as long as the gain per stage, Z_g/Z_o, is appreciable ($\gg 1$), the prototype of Fig. VI-15 is an adequate approximation (for most practical gap lengths)

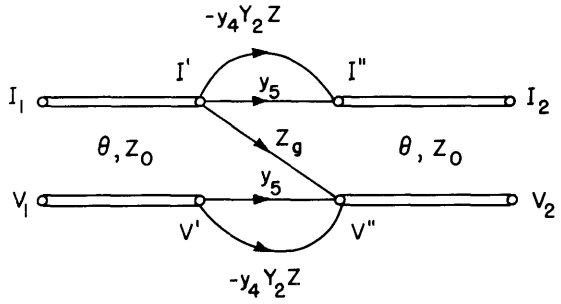

Fig. VI-15. Approximation to the flow graph of Fig. VI-14: prototype of multicavity-klystron structure.

to the prototype of Fig. VI-14. Accordingly, Eq. 10 becomes

$$\left.\frac{I_2}{V_1}\right|_{I_1=0} = \left(Y_o^2 \sin^2\theta\, M^2 Z + jY_o \sin^2\theta\right) e^{-j\theta g} \qquad (11)$$

$$-jY_o \sin 2\theta\, y_4 Y_2 Z$$

Further evaluation of the effect of a finite gap is in progress.

A. Bers

References

1. A. Bers, Quarterly Progress Report, Research Laboratory of Electronics, M.I.T., Oct. 15, 1956, pp. 34-36.
2. L. D. Smullin, A. Bers, H. W. Fock, and A. H. Czarapata, Quarterly Progress Report, Research Laboratory of Electronics, M.I.T., April 15, 1957, pp. 47-50.
3. A. Bers, Quarterly Progress Report, Research Laboratory of Electronics, M.I.T., Jan. 15, 1956, p. 55.

3. Design: Hollow-Beam Klystron

The parts for the seven-cavity, stagger-tuned, hollow-beam klystron, described in the Quarterly Progress Report of April 15, 1957, page 47, are being designed and cold-tested. The exact dimensions for the intermediate cavities have been determined, and the corresponding parts are being constructed.

The output cavity must have an extremely low Q, $Q_L \approx 7$, in order to pass the frequency band of the preceding interaction structure. The conventional method of loading the cavity by overcoupling with a large loop was unsuccessful. Cold tests have been completed on a type of output coupling, as shown in Fig. VI-16. A loaded Q of $Q_L \approx 7.5$ was obtained on a scaled-down model. A full-scale output cavity of this type, together with a coaxial output transmission line and an output vacuum seal (See Fig. VI-17), is

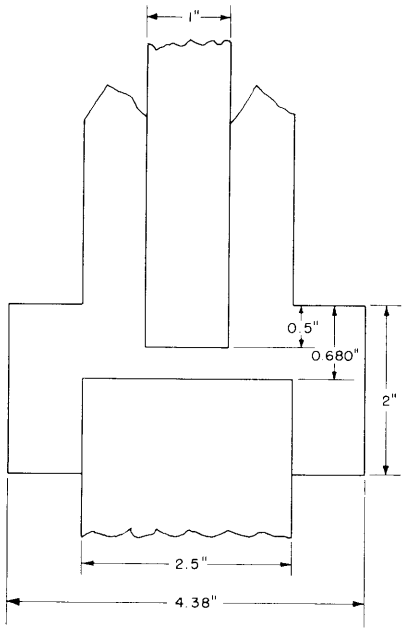

Fig. VI-16. Output interaction gap.

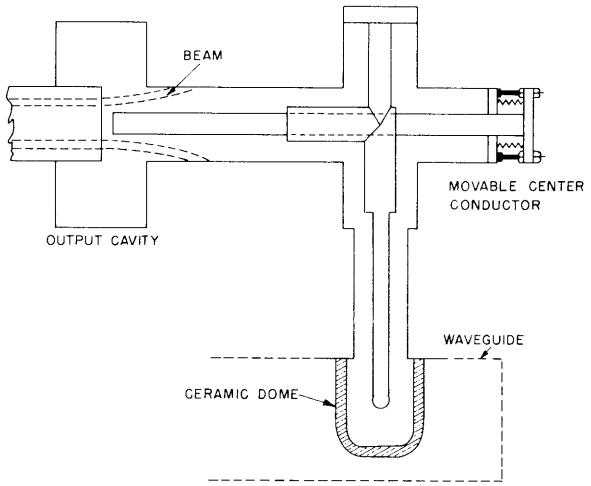

Fig. VI-17. Output structure.

being designed and will be tested for its frequency response.

The input cavity must have the same Q as the intermediate cavities, i.e., $Q_L = 20$. The gap length of the input cavity is only half that of the intermediate cavities, in order to reduce the velocity modulation that will appear at the following gap. But, with the shorter gap, the electronic beam loading is so greatly reduced that the input cavity has to be loaded by overcoupling of the input line. Cold tests are being made on coupling systems that may yield the necessary degree of coupling and still not disturb the radial symmetry of the gap field excessively.

The gun design is being checked for minor improvements.

H. W. Fock